KERNFORSCHUNGSZENTRUM

KARLSRUHE

Juli 1975

KFK 2205
AEEW-R 987

Institut für Reaktorentwicklung
Projekt Schneller Brüter

A Comparison of Temperature Distributions Calculated by the SABRE Programme with Experimental Results

R. Herbert
Atomic Energy Establishment Winfrith, Dorchester, Dorset

D. Kirsch
Gesellschaft für Kernforschung mbH, Karlsruhe

GESELLSCHAFT
FÜR
KERNFORSCHUNG M.B.H.

KARLSRUHE

GESELLSCHAFT FÜR KERNFORSCHUNG M. B. H.

KARLSRUHE

KERNFORSCHUNGSZENTRUM KARLSRUHE

KFK 2205
AEEW-R 987

Institut für Reaktorentwicklung

Projekt Schneller Brüter

A COMPARISON OF TEMPERATURE DISTRIBUTIONS CALCULATED BY THE SABRE PROGRAMME WITH EXPERIMENTAL RESULTS

R. Herbert*
D. Kirsch**

Gesellschaft für Kernforschung mbH, Karlsruhe

---

*Atomic Energy Establishment, Winfrith, Dorchester, Dorset
**Institut für Reaktorentwicklung

ABSTRACT

A joint effort has been undertaken by AEE Winfrith and GfK/IRE Karlsruhe to compare temperature distributions in the wake downstream of a blockage in rod bundles. Such temperature distributions on one hand have been measured in Karlsruhe and on the other hand can be calculated using the SABRE code developed for Winfrith under a contract placed at Imperial College, London. A brief description of the experiments and of the SABRE code are given in this report as well as detailed measurement and calculation results. It is concluded that this code is already a very useful tool for safety investigations for L.M.F.B.R.s, despite the fact that some parameters used are not very well known and that improvements to the code may be necessary.

ZUSAMMENFASSUNG

Ein Vergleich von mit dem SABRE-Programm berechneten Temperaturverteilungen mit experimentellen Ergebnissen.

Als ein gemeinsames Unternehmen von AEE Winfrith and GfK/IRE Karlsruhe wurden Temperaturverteilungen im Totwasser hinter Blockaden in Stabbündeln verglichen. Solche Temperaturverteilungen wurden einerseits in Karlsruhe gemessen und können andererseits mit dem SABRE-Programm berechnet werden, das für Winfrith gemäss einem Vertrag mit London, entwickelt wurde. Eine kurze Beschreibung der Experimente und des SABRE-Programms werden in diesem Bericht gegeben, ebenso auch detaillierte Meß- und Rechenergebnisse. Trotz der Tatsachen, daß einige der im Programm zu benutzenden Parameter nicht sehr gut bekannt sind, und daß Verbesserungen des Programms als notwendig erkannt werden, wird geschlossen, daß dieses Programm auch jetzt schon ein sehr nützliches Hilfsmittel fur Sicherheitsuntersuchungen für flüssigmetall-ge-kühlte schnelle Brutreaktoren ist.

CONTENTS

TABLES

FIGURES

1. INTRODUCTION

In the field of safety investigations for liquid-metal cooled fast breeder reactors (LMFBRs), local coolant disturbances are studied as initiating events for self-propagating damage to the core (1) (2). Several possible mechanisms of failure propagation have been considered. The most important one could be initiated by a local coolant blockage within an individual subassembly, which may arise from an accumulation of fuel particles or other coolant impurities at the spacer grids of the rod bundle. Local coolant blockages may not be detected by temperature sensors or flowmeters at the subassembly outlet before a critical situation, such as local sodium boiling and/or progressive fuel pin failure, is reached.

Because of the assumption that these blockages are generated by the deposition of small particles at a spacer grid, blockages are considered which are small axially but possibly large radially. Furthermore the rod bundle geometry near the blockage is assumed to be undisturbed, since with a disturbed geometry one has to expect an early clad failure so that a blockage can probably be detected, eg from the release of fission gas.

Under these assumptions one has to investigate the temperature distribution for a single-phase flow downstream of a local coolant blockage to get the initial conditions for a possible failure propagation. This has been done recently in two different approaches:

(i) In the UK a new computer code SABRE (= Subchannel Analysis of Blockage in Reactor Elements) has been developed at Imperial College under the terms of a contract between UKAEA, Winfrith, and Combustion, Heat and Mass Transfer Ltd (CHAM). The SABRE code is devised to treat blockage situations in rod-cluster geometries, where large cross flows and a recirculating wake require a three-dimensional solution of the elliptic differential equations of conservation of mass, momentum and energy (3). So far no other code has treated successfully such problems for large blockages in rod bundles of reactor size.

(ii) In Germany temperature distributions downstream of large blockages have been measured at KFK/IRE in a full-scale mock-up of a fuel subassembly in a water test rig. From the temperatures measured in water flow the sodium temperatures have been calculated. This has been justified (4) when the Reynolds number is sufficiently high and the blockage sufficiently large. No other experiments are known to measure temperature distributions downstream of large blockages in rod bundles of reactor size.

Although the SABRE code is still in a state which requires further improvement, it was considered useful to calculate the KFK experiments with it and to compare experimental and theoretical results. Therefore, a joint effort was undertaken by AEEW and KFK to undertake this comparison, the results of which are given in this report.

2. EXPERIMENTAL INVESTIGATIONS OF TEMPERATURE DISTRIBUTIONS IN THE RECIRCULATION ZONE

2.1 Test Facility and Instrumentation

To measure the temperature distributions downstream of local coolant blockages in rod bundle subassemblies, a full-scale mock-up of an SNR-fuel subassembly (5) was constructed (Figure 1). The SNR subassembly consists of a hexagonal array of 169 fuel rods with a diameter of 6 mm and a pitch of 7.9 mm. The fuel rods are replaced by electrically heated rods of 1.0 m total length with a heated length at the downstream end of 0.7 m (0.1 m upstream and 0.6 m downstream of the blockage) and a maximum rod power of 50 W/cm, which is nearly constant over the heated length. This test section was inserted into a water test rig with a maximum water flow rate of 100 m^3/h. The water of the rig can be preheated to a maximum temperature of 90°C.

Figure 1 shows a central, symmetrical blockage inserted in the rod bundle, which obstructs 15% of the total flow area. Due to the thermocouples downstream of the blockage no grid spacers could be inserted in this region, ie the axial arrangement of the spacers is not quite the same as in the SNR. The blockage consists of two 4 mm thick metallic discs separated by a rubber disc as a seal.

Several rods in the middle of the bundle are provided with three thermocouples each, which in the wake region are placed in slots in the heater cladding in order not to disturb the flow. Since the cladding thickness amounts to only 0.45 mm, thermocouples of 0.25 mm outer diameter had to be used. The thermocouple hot junctions are bent out of the cladding into the middle of the subchannels. The thermocouple distribution was chosen in such a way that the temperature field in the wake could be measured as comprehensively as possible, ie in different axial planes and in as many subchannels as possible, taking advantage of the symmetry of the assembly. Because of limitations in the instrumentation and data evaluation (number of amplifiers available etc.) the total number of thermocouples was limited. Therefore, with large blockages only a part of the temperature field in the wake could be measured. Another limitation is imposed by the fact that some of the thermocouples failed because of the difficulty of mounting such small thermocouples. The actual location of the active thermocouples is given together with the experimental results (see Section 2.4).

2.2 Data Evaluation

The time for the measurement of the steady-state (because the flow is turbulent, this is actually a quasi-steady-state) temperature distribution is limited by the design of the water test rig used. With the highest possible flow rate (100 m^3/h) there are only about 20 sec between the moment when steady-state conditions are reached after switch-on of the heaters, and the moment when the inlet temperature begins to rise and the temperature distribution becomes unsteady again. Therefore, a fast multi-channel data acquisition device was necessary in order to record sufficient data for an

adequate calculation of the time mean value for each thermocouple. This device scans all thermocouples cyclically for 8 secs with a cycle time of 10 milliseconds, digitalizes the instantaneous values of the analogue data and stores them sequentially on a magnetic tape. These 800 measurements are sufficient for the calculation of the time mean value. This has been shown by an evaluation with shorter measurement times (ie fewer data). The time mean value changes slightly with measurement times less than 4 sec but does not change with measurement times of more than 4 sec.

The magnetic tapes have been evaluated on an IBM/370-165 computer using the code system SEDAP (6). SEDAP reads the measurements and sorts them into time dependent signals for each thermcouple, at the same time converting the thermocouple voltages into temperature differences. An analysis of the time dependent signals is possible using SEDAP, but in this case only the time mean value is of interest. This is also calculated by SEDAP.

2.3 Measurement Errors

Using SEDAP an evaluation method has been found which is independent of the reference temperature of the thermocouples (ambient temperature), and which practically eliminates the error in the recording of the rather small absolute values of the thermocouple voltages and the error due to the temperature drift of the amplifiers' zero adjustment. The error in the amplification factor could not be eliminated and this leads to an uncertainty of the resulting temperature differences which amounts to $\pm$ 2%.

The resistance of the electric heaters and, therefore, the rod power is slightly different for different rods. This leads to another possible uncertainty of $\pm$ 3% for the temperature differences. An error in the measurement of the total power does not lead to an error in the temperature differences, since the total power was not in the data evaluation. However when considering calculations with the SABRE code one has to take account of this error, ie the power given as input for SABRE is known only to within 1.5%.

All thermocouples will show a temperature, which is slightly higher than the water temperature to be measured because of heat conduction from the heater cladding through the thermocouple sheath to the thermocouple junction. An estimate with a subchannel velocity of 2 m/s and maximum rod power gives the result, that the measured temperature is 0.2°C higher than the water temperature. The high turbulence intensity in the wake will tend to decrease this figure, on the other hand a time mean velocity of 2 m/s is not reached at all points of the wake. Thus an adequate figure for this error cannot be given.

The flow rate through the test bundle could be measured only to within $\pm$ 4%, which leads to an uncertainty of the same value in velocity and Reynolds Number, but has no influence on the temperature differences.

Some other possible sources of error have been discussed in the original report on the first experiments (7) which concludes that these errors can be neglected when compared with the errors mentioned here.

Summing up all errors for the temperature measurement one has to conclude that an overall figure for the error in the temperature differences can hardly be given. It is only a rather rough estimate if one assumes an error of ± 5% of the temperature differences given as results, and one has to point out that this error may be increased for certain thermocouples due to their locations in the wake, and that the measured temperature generally tends to be a few tenths of a ^{o}C higher than the water temperature.

For the calculation of the experiments with the SABRE code one has to take account of an uncertainty of 1.5% in the total power and of ± 4% in the inlet velocity.

2.4 Experimental Results

Temperatures downstream of three different blockages 1 cm thick have been measured so far, one of them obstructing about 15% of the flow area in a central symmetrical position (see Figure 1), the second obstructing about 41% in the same position, and the third obstructing about 47% of the flow area in a corner of the hexagonal assembly. With each of these blockages measurements have been made with different flow rates and inlet temperatures (ie for different Reynolds Numbers). A summary of the experimental data is given in Table 1.

For each blockage two measured temperature difference distributions are given in Table 2 to Table 7 as examples of different conditions. The temperature difference given there is the difference between the measured temperature of the thermocouples in the specified location and the inlet-temperature. The subchannel is specified by giving the numbers i and j corresponding to the respective numbers with the SABRE-calculation (see Figures 4 and 5). It must be stated at this point that the actual thermcouple location is given by i,j only within the symmetry for the respective case, ie hexagonal symmetry for the central blockages and mirror symmetry for the edge blockage.

3. THE SABRE PROGRAM

3.1 Basis of the Method

SABRE is a computer program for the Subchannel Analysis of Blockages in Reactor Elements. It is a logical step forward from (but not development of) pre-existing subchannel analysis codes such as HAMBO (10), and COBRA (11), and others because it is not subject to the formerly overriding restriction that flows had always to have a single dominant direction, such that flows transverse to this direction were small relative to the dominant flow. That is, the calculation of recirculating flows was not allowed. In SABRE this restriction is removed so that the recirculating flows which can occur

down - and upstream of a blockage in an assembly of subchannels may be calculated.

The SABRE method is a development of a general method (12, 13, 14) of calculating steady or time dependent flows flows in three dimensional continua with distributed or local resistances and heat sources, and with physical properties varying with the physical conditions. The basis of the general method is an algorithm called SIMPLE (Semi-Implicit Method for Pressure Linked Equations). In this method the calculational zone is divided into cells by means of rectangular grids of variable spacing. The velocities (averaged over the faces) of the fluid entering and leaving each cell are related to the temperature and pressure in the cells, due account being taken also of diffusion effects. In principle the general method could be applied directly by sufficiently subdividing the subchannels and representing the rods as solid boundaries within the domain of calculation, although at present it is not felt that adequately representative expressions for momentum fluxes are possible in such geometry. This however would only be possible for the smallest of problems with the present state of computer technology, because both storage requirements and computing time would be prohibitively large. Therefore in the SABRE program the calculational cells are the subchannels, divided along their length into sections of variable length. (A subchannel is the space between 3 or 4 rods on a triangular or square lattice respectively). It then becomes necessary to augment the equations of conservation of mass, momentum, and energy by non-linear empirical correlations describing the resistance of the subchannels and the passages between them to the flow of fluid. The non-linearity of these relations tends to decrease the rate of convergence of the solution procedure and SABRE is therefore confined at this stage to steady state single phase flows in which physical properties vary only within fairly narrow limits, thus the overall non-linearity of the equation set is kept to a minimum. The development to a transient version is, however, thought to be a relatively simple extension. The progression to two-phase conditions must await the devising of suitable and appropriate models of two-phase flow in rod bundles. The numerical techniques and physical approximations embodied in the code are outlined in the Appendix.

3.2 Scope of the Program

The restriction to single-phase steady state flow has already been mentioned and to some extent justified. The object of this section is to describe the type of problems which can be solved with the SABRE program.

The program was written for close-spaced rod bundles arranged on a triangular lattice (for the definition of the term close, see Section A3 of the Appendix) and account was taken of the desirability of including square lattices later. For the triangular case the subchannels are divided as shown in Figure 2. The pressure and temperature averaged over the control volume are considered to act at the centre of that volume which is connected with its neighbours by flows with velocities (components u, v, w) averaged over appropriate

faces of the control volume and by heat fluxes. The transverse (u and v) velocities are calculated with the aid of secondary control volumes shown in section in Figure 3, and the physical properties which determine the axial (ie w) velocities are averaged over the cell shown in broken lines in Figure 2. Deviations within limits from the nominal pin size and position are allowed for by corrections to the nominal areas and wetted perimeters of the control volumes. The limitations are that the pin must not leave (by swelling or bowing) the hexagonal cell of the unperturbed lattice which originally contained it, and it must not shrink sufficiently to invalidate the close spacing approximation.

The lateral boundary subchannels have their own special geometrical treatment, and almost any shape of physical boundary is allowable, or the boundary conditions may be of prescribed flow or pressure, so that a sector of rotationally symetric problem may be treated. The flow, pressure, and temperature boundary conditions may be specified in any self consistent manner. The usual axial boundary conditions are either prescribed inlet flow to the subchannels or of prescribed pressure at inlet and outlet. This is not however a fundamental restriction.

The rods may be in reality spaced by periodical grids or by spiral wire wraps. The representation of grids by additional flow resistances presents only problems of program organisation, as there is at present no indexing scheme included to identify grid locations and this would increase storage requirements. Thus the grids present in the experimental assembly were not represented in the calculations described in this report. Wire wrap spacers present much more serious difficulties as they tend to induce flow circulation around the pins.

4. COMPARISON OF CALCULATIONAL RESULTS WITH EXPERIMENTAL DATA

4.1 Computation Requirements and Calculated Cases

Since the SABRE code needs storage for all main variables (three velocity components, pressure, enthalpy etc.) at all grid nodes and 100 or more iterations for an approach to the final solution, a rather large core store and a long computing time is required for the calculation of the experiments. Although advantage was taken of the symmetry of the cases, a core store of approximately 700 K bytes for the central symmetrical blockages and 1500 K bytes for the edge blockage has been required on an IBM/370-165 computer. This core store is necessary for 52 (15% blockage) and 55 (41% blockage) axial intervals with the 64 subchannel arrangement (see Figure 4) of the central symmetrical blockages, and for 70 axial intervals with the 192 subchannel arrangement (see Figure 5) of the 47% edge blockage. The computing (CPU) time required to reach a sufficiently converged solution was 10 minutes for the 15% blockage, and 30 minutes for the 41% blockage. As a measure of convergence the sum of mass sources (see Appendix Section A3) was taken. This is given for all calculational results in Tables 8 to 12. For the 47% edge blockage case, a sufficiently converged solution could not be reached within a computing time of 160 minutes. The

computation was stopped when the value for the sum of mass sources did not decrease further with additional iterations, but oscillated slightly around a fixed value. Since the values for the calculated variables (especially the temperature) are nearly constant in this stage, it may be concluded that the solution reached is not far from the final solution; this is supported by experience with other similar cases.

Because of the core store and computing time required most of the calculations have been performed for the 15% central, symmetrical blockage. Three experiments (15.01, 15.04 and 15.10) with this blockage have been calculated using nominal calculational parameters, and the effect of variation of the important calculational parameters was studied for these cases only. Only one experiment was calculated, with nominal calculational parameters, for the 41% central blockage (Exp. No. 41.01) and 47% edge blockage (Exp. No. 47.01), respectively.

4.2 Choice of Axial Mesh Size, Especially for the Wake Region

Since it was known from earlier SABRE calculations, that flow and temperatures in a wake region are rather strongly dependent on the choice of the axial mesh size, whereas flows and temperatures in other ("undisturbed") regions are not very sensitive to this choice, the first calculations were done to find an appropriate axial mesh size for the SNR-geometry (5), which had to be represented in the calculations. Table 8 shows the result of calculations of Exp. No. 15.04 for three different axial mesh sizes in the wake region. As can be seen from the results given in Table 8 the calculated temperature differences are generally lower than the measured ones (except four out of 27 values for 5 mm axial mesh size and one out of 27 for 10 mm mesh size). Nevertheless the overall shape of the measured temperature distribution seems to be represented reasonably well by the SABRE results.

Comparing the results for different mesh sizes one can see, that the medium mesh size used (5 mm) leads to the highest calculated temperature differences and to a fairly close agreement between measured and calculated values. Therefore for all other calculations the axial mesh size in the wake region was fixed at 5 mm. The wake region in this sense includes not only the wake itself, but also a region of 15 mm upstream of the blockage and 20 mm downstream of the wake, the extension of which is known from other experiments (4). Beyond the wake region on both sides a region of 10 mm axial mesh size follows, and the mesh size is further increased to 20 mm and finally 50 mm at both ends of the 1 m long rod bundle. The calculation is confined to the length of the rod bundle. It should be noted here, that 5 mm axial mesh size is comparable to the linear dimension of the subchannel cross section, the hydraulic diameter of which amounts to 5.3 mm.

4.3 Calculation of Basic Cases with Nominal Parameters

For the calculation of the experiments the geometry of the test bundle (see Section 2.1 and Figure 1), has been given as input data for the SABRE code in the form shown in Figures 4 and 5, taking advantage of the symmetry. Due to a misunderstanding the axial height of the blockage was given as 5 mm for the calculations, compared with the actual value of approximately 10 mm in the test section, but this mistake has no great influence on the results. Grid spacers could not be represented in this version of the SABRE code.

Input data for power distribution and inlet temperature were taken from the measured experimental values (see Table 1) as was the prescribed flow rate at bundle inlet. Other nominal parameters (eg friction factors, eddy diffusivities of momentum and heat) were taken as they were, included in the then current version of the SABRE code (see Appendix A4) on the basis of experience with earlier calculations.

With this set of nominal parameters and those given in Section 4.1 and 4.2 the Experiments 15.01, 15.10, 41.01 and 47.01 have been calculated. The calculated temperature differences are given in Tables 9, 10 and 11 for those locations, for which thermocouple readings exist so that the values given there can be compared directly with the measured values given in Tables 2, 3, 4 and 6. More calculated values for three different axial planes downstream of the blockage are given in Figures 6, 7 and 8 together with measured values for comparison.

This comparison yields the following results:-

(i) 15% central, symmetrical blockage

As already mentioned in Section 4.2, the calculated temperature differences tend to be generally slightly lower than the measured ones, but the shape of the temperature distribution is represented fairly well by the calculated results. The maximum temperature in the wake is found immediately downstream of the blockage near its edge, which is in agreement with the experimental results. This can be explained from the flow pattern, the coolant being heated up further when flowing radially from the centre of the blockage to its edge. In the core of the quasi-stationary eddy, which is located 30 to 40 mm downstream of the edge of the blockage, no marked increase in temperatures is observed, though the time mean velocities are very low here, but this can be explained by the intense turbulent mass exchange with the main flow. The maximum calculated temperature in the wake is only slightly higher than the maximum given in Table 9 and Figure 6. It is found 2.5 mm downstream of the blockage in subchannel 5, 3. The temperature rise relative to the inlet temperature amounts here to 13.5°C for the calculation of exp. no. 15.01 (compared with 13.1°C at Location 5,3 and 10 mm given in Table 9 and Figure 6.

(ii) 41% central, symmetrical blockage

Again the calculated temperature differences tend to be generally lower than the measurements, while the shape of the temperature distribution is represented fairly well. But in this case the maximum calculated temperatures in the wake are found in the core of the eddy, which for this blockage is located 40 to 50 mm downstream of the edge of the blockage. The maximum calculated temperature difference is found in subchannel 7,3, 50 mm downstream of the blockage, and amounts to 22.3°C (compared with 20.6°C at location 6,3 and 40 mm given in Figure 7). Unfortunately only a few measured temperatures are available in the region of the core of the eddy (left hand side of Figure 7), but these values do not confirm the calculated temperature maximum. There is thus a disagreement between the code and experiment which cannot at this stage be resolved, over the position of the temperature maximum in the wake behind larger blockages.

(iii) 47% edge blockage

In this case the greatest differences between measured and calculated values are found. For the temperature profile on the x^+- axis (see Figure 8) 10 mm downstream of the blockage, where ample experimental values are available, the increase in temperature towards the edge of the blockage is much steeper for the measured than for the calculated profile. The maximum calculated temperatures in the wake are again found in the core of the eddy which is 50 to 60 downstream of the blockage. The maximum calculated temperature difference is found 55 mm downstream of the blockage in Subchannel 12,2, and amounts to 48.6°C (compared with 34.9°C at Location 12,2 and 40 mm given in Figure 8). In this case no temperature measurements in the core region of the eddy are available (some thermocouples had been inserted here, but showed abnormal behaviour, so that the results from these thermocouples could not be evaluated). Therefore, the high temperatures calculated in this region, which are much higher than any measured temperatures (in contrast to the 41% central blockage case), remain unconfirmed.

4.4 Variation of Important Calculational Parameters

A series of six calculations of Exp. No. 15.01 has been performed, in which the more important calculational parameters have been varied in the following ways.

(i) Total (ie molecular + turbulent) thermal diffusivity set to zero ($\Gamma_H = \lambda/c_p + \rho\varepsilon_H = 0.0$)*

* λ: thermal conductivity, c_p: specific heat, ρ: density, ε_H: eddy diffusivity of heat.

(ii) Total thermal diffusivity set to a constant arbitrary value (Γ_H = 0.1 kg m^{-1} s^{-1}).

(iii) Axial friction factor halved.

(iv) Axial friction factor doubled.

(v) All friction factors halved.

(vi) All friction factors doubled.

The results of these calculations are summarized in Table 12 together with the results of the nominal recalculation of Exp. No. 15.01. The influence of the variations of calculational parameters on the results is as follows:-

(i) and (ii). A variation of the total thermal diffusivity Γ_H has almost no influence on the calculated temperature distribution. The values calculated for Γ_H = 0 and Γ_H = 0.1 (= constant) are practically unchanged from the normal case, which is calculated with a total thermal diffusivity varying from node to node depending on the flow and turbulence conditions. This surprising result can be explained by a false heat transport, which originates from the substitution of the heat transport differential equations by the finite-difference equations (see Section 5.2). To the extent that this problem has not been solved in a satisfactory way, SABRE results must be considered preliminary.

(iii) and (iv). The calculated temperature distribution is strongly influenced by a variation of the axial friction factor. With increased axial friction factor the calculated temperatures in the wake decrease, and vice-versa. A detailed examination of the calculated results showed that this behaviour can be explained by the fact that the calculated extent of the wake is influenced by the axial friction factor. It decreases with increasing axial friction factor and vice-versa since axial friction factors in rod bundles are well-known the influence of axial friction can be taken into account with reasonable confidence except in the wake.

(v) and (vi). The effect of a variation of the lateral friction factors (which are equal in x- and y-direction) is negligible within the range of variation investigated.

4.5 The Flow Field

Using nominal thermal and hydraulic parameters SABRE produces velocity distributions which qualitatively agree well with the experimental patterns reported in (4). This holds for all three blockages investigated. In particular, for the 47% edge blockage, the secondary vortex found downstream of the blockage in the corner between the blockage and

subassembly wall is predicted by SABRE, and the predicted extent of this vortex agrees well with that found experimentally. Since SABRE predicts another vortex with flow reversal in the corresponding corner upstream of the 47% blockage, the high-speed films of the flow visualisation experiments were re-examined in an attempt to find this vortex. However the velocities upstream of the blockage are too high to permit determination of the flow direction in the region in question. Thus the SABRE calculations cannot be confirmed in this region.

A comparison of absolute values of the velocity could not be made, since these values were not measured in the experiments.

5. DISCUSSION AND CONCLUSIONS

5.1 Adequacy of the Experiments for a Test of the SABRE Code

For a test of SABRE calculations of the temperature distribution in the wake downstream of a blockage in a rod bundle a comparison was needed with experimental results from a full bundle with various large blockages. However there are only a few experiments reported in which temperature distributions in rod bundles downstream of blockages have been measured. Schleisiek (8) has measured the temperatures downstream of a blockage in an annular subchannel geometry (only a "two-dimensional rod bundle") in sodium as well as in water. Fontana et al. (9) used real rod bundles for their measurements, but the maximum number of rods was restricted to 19, and moreover they used wire-wrap spacers which cannot yet be treated with the SABRE code, and are not intended to be used in British or German Fast Breeder Reactors at this time.

Thus only the experiments reported by Kinsel (4) and briefly described in Section 2 appear suitable to test the capability of the SABRE code. Unfortunately only temperature measurements not velocity measurements could be made in these experiments. However the temperature measurements seem to be a sufficient basis for a comparison to test the SABRE code since the temperatures depend on the flow pattern.

Nevertheless one has to remember for this comparison that not only the SABRE results, but also the measurement data may be affected by errors. For various reasons, which are explained in Section 2.3, a general figure for the uncertainty of the temperature measurements cannot be given, but it has been concluded that in spite of this it is improbable that the experimental results suffer from such serious uncertainties as would render them useless.

Important new ideas for future experiments have been suggested by the calculations, the most important being to insert more thermocouples into the core of the eddy, especially with large blockages.

5.2 Adequacy of the SABRE Version Used for the Comparison

The version of SABRE used for this study was in two senses preliminary. Firstly, in the contract for the

development of the program the specification of input and output facilities was that they need be no more than the minimum necessary for the development of the basic method. The data input is therefore in need of rationalisation and improvement to enable easy passage from one case to another, which at present requires some reprogramming. The output is at present in the form of tables, plane by plane of each of the five variables velocity (u, v, w), pressure and temperature. While a subsidiary program exists to produce fields of vectors representing velocities in planes, this falls a long way short of giving a fully 'three-dimensional' appreciation of the results to the user.

The current version is also provisional in the sense that, while the friction and turbulent diffusivity data are an assembly from various sources of the best available data, they are not all of proven applicability in the rod bundle situation. In spite of the fact that this study to some considerable extent verifies the applicability of some of the data, there is still much scope for improvement, particularly for the case of flows which are far from being either parallel or perpendicular to the rods.

The second shortcoming is more fundamental to the method itself and has the name of 'false diffusion'. This is an effect introduced by the finite difference techniques necessary for the formulation of the equations in the SIMPLE form. It occurs when the flow is in a direction oblique to the mesh. It results in the false diffusion of properties particularly enthalpy, to neighbouring points which physically in purely convective flow, should not 'see' the properties of the original point, but which are taken into account as neighbours of the calculational point being considered. In the general method, as applied to continua it may be reduced to acceptably small proportions by the use of small mesh intervals and orienting the mesh lines along the directions of any dominant flows which may be present. This method, which is not always effective, for example in a recirculating zone, is not applicable to the subchannel model of SABRE, because the lateral mesh is defined by the rods. Correct choice of axial mesh is important for regions of oblique flow, as this study has shown, and the choice of a minimum axial division approximately equal to the hydraulic diameter of the subchannels seems plausible. Research continues both at AEE Winfrith and at Imperial College to reduce the effects of false diffusion, which may account for most of the discrepancy between the calculations and experiment.

Besides the reduction of the false diffusion effect, which continues, future work on SABRE to remove the restriction to steady state conditions and to include two-phase effects has been contemplated. The extension to deal with single-phase transient problems is in principle quite simple, because the convergence of the SIMPLE procedure is in many respects similar to the development of the flow with time from the initially guessed conditions to the final steady state. The inclusion of two-phase phenomena is however, a much more difficult problem for two reasons. First, as yet no adequate mathematical model exists to describe two-phase flow in rod

bundles at near atmospheric pressures. The second, and perhaps more serious difficulty is that from the present knowledge of this SIMPLE technique, it may be predicted that the gross changes of physical properties accompanying phase change would make convergence much slower and more difficult to procure. This is because the rate of convergence depends on the non-linearity of the equation set. It must not, however, be thought that a two-phase version is not possible, but it will surely be difficult to realise without the development of new numerical procedures, even given a good physical model for the rod bundle situation.

The poor convergence of the 47% blockage case can, it is believed, be attributed to an error in the double sweep - block adjustment procedure which has since been found and corrected at AEE Winfrith. This has resulted in faster and better convergence for cases similar to the 15% and 41% blockage cases. The 47% blockage case has not been retried at the time of writing.

5.3 Conclusions

As has been shown by the comparison reported here, the SABRE code in the version used calculates the temperature distribution in the wake downstream of a blockage in a rod bundle in such a way that the shape of the measured temperature distribution is represented fairly well by the calculated results, whereas the absolute values of the results tend to be slightly too low. This statement relates to cases for which nominal hydraulic and thermal parameters are used, and is most appropriate for blockages which are not too large.

In spite of the fact that some of the "nominal" parameters are not well known and that improvements of the SABRE code are known to be necessary, it is concluded that this code is a very useful tool for safety investigations for LMFBRs even in its present form. If for such investigations a conservative approach for the temperature distribution in the wake of a blockage is to be calculated (ie a temperature distribution, which is higher than the actual one), one may use the SABRE code for this calculation with nominal parameters except the axial friction factor, which may be decreased.

ACKNOWLEDGEMENTS

The authors wish to acknowledge the assistance given by Mrs M G Staniforth and Dr D Blackburn with the calculations, and the co-operation of the computer staff, who made it possible to do so much work in such a short time.

REFERENCES

1. GAST, K., SMIDT, D. Cooling Disturbances in the Core of Sodium-Cooled Fast Reactors as Causes of Fast Failure Propagation, Nucl. Eng. Design 14 (1970) 12-22.

2. GAST, K. Die Ausbreitung örtlicher Störungen im Kern Schneller Natriumgekuhlter Reaktoren und ihre Bedeutung für die Reaktorsicherheit, KFK 1380 (1971).

3. GOSMAN, A. D., HERBERT, R., PATANKAR, S. V., POTTER, R., SPALDING, D. B. The SABRE Code for Prediction of Coolant Flows and Temperatures in Pin Bundles containing Blockages, Paper No. 82, Intern. Meeting on Reactor Heat Transfer, Karlsruhe 1973.

4. KIRSCH, D. Untersuchungen zur Stromungs - und Temperaturverteilung im Bereich lokaler Kühlkanalblockaden in Stabbundel - Brennelementen. Dissertation Universität Karlsruhe (TH)/KFK 1794 (1973).

5. GAST, K., SCHLECHTENDAHL, E. G. Schneller Natriumgekühlter Reaktor Na 2, KFK 660 (1967)

6. AUDOUX, M., KATZ, F. W. OLBRICH, W. SCHLECHTEN-DAHL, E. G. SEDAP - An Integrated System for Experimental Data Processing KFK 1594 (1973).

7. GRÖTZBACH, G. Messung der Temperaturverteilung im Totwasserbereich lokaler Blockaden in einem Brennelementmodell, Diplomarbeit Universität Karlsruhe (TH) (1972)

8. SCHLEISIEK, K. Natriumexperimente zur Untersuchung lokaler Kühlungs-storungen in brennelementähnlichen Testanordnungen, Dissertation Universitat Karlsruhe (TH)/KFK 1914 (1974).

9. FONTANA, M. H. et al. Effect of Partial Blockages in Simulated LMFBR Fuel Assemblies. ORNL-TM-4324, 1973.

10. BOWRING, R. W. HAMBO: A Computer Programme for the Subchannel Analysis of the Hydraulic and Burnout Characteristics of Rod Clusters. Part I - A General Description, AEEW - R 534.

11. ROWE, D. S. (1971). "COBRA III. A Digital Computer Program for Steady State and Transient Thermal Hydraulic Analysis of Rod Bundle Nuclear Fuel Elements". BNWL-B-82.

12. PATANKAR, S. V. and SPALDING, D. B. (1972). "A Calculation Procedure for Heat, Mass and Momentum Transfer in Three-Dimensional Parabolic Flows." International Heat and Mass Transfer, Vol. 15 pp 1787-1806.

13. CARETTO, L. S., GOSMAN, A. D., PATANKAR, S. V. and SPALDING, D. B. "Two Calculation Procedures for Steady Three Dimensional Flows with Recirculation". Proceedings of the Third International Conference on Numerical Methods in Fluid Mechanics, Springer Verlag, 1972.

14. PATANKAR, S. V. and SPALDING, D. B. (1972). "A Calculation Procedure for the Transient and Steady State Behaviour of Shell and Tube Heat Exchanger." Imperial College, Mechanical Engineering Department Report HTS/72/6.

15. REHME, K. (1972). "Pressure Drop Performance of Rod Bundles in Hexagonal Arrangements". Int. J. Heat and Mass Transfer, 15, pp 2499-2517.

16. McADAMS, W. H. (1954). Heat Transmission. McGraw Hill, 3rd Edition.

17. NIJSING, R. and EIFLER, W. (1971). 'Temperature Fields in Liquid Metal Cooled Assemblies.' Proc. International Seminar on Heat Transfer from Liquid Metals, Trogir Yugoslavia.

Table 1: Summary of main experimental data

No. of experiment	type of blockage x)	flow rate m^3/h	inlet velocity m/s	total power kW	inlet temperature °C	total coolant temp. rise (measured) °C
15.01	1	40	2.348	549	23.6	11.68
15.02	1	60	3.521	549	25.0	7.94
15.03	1	80	4.695	549	25.4	6.01
15.04	1	40	2.348	548	62.0	11.55
15.05	1	60	3.521	550	63.2	8.00
15.06	1	80	4.695	546	64.0	5.78
15.07	1	100	5.869	548	64.6	4.81
15.08	1	60	3.521	544	89.6	7.36
15.09	1	80	4.695	540	90.7	6.44
15.10	1	100	5.869	549	90.2	4.78
41.01	2	40	2.348	559	24.1	12.74
41.02	2	60	3.521	559	24.8	8.45
41.03	2	80	4.695	559	25.7	6.45
41.04	2	40	2.348	559	60.0	12.92
41.05	2	60	3.521	559	60.6	8.40
41.06	2	80	4.695	559	61.2	5.79
41.07	2	60	3.521	559	74.8	8.48
41.08	2	80	4.695	559	76.0	6.15
41.09	2	100	5.869	559	76.2	5.63(?)
47.01	3	40	2.348	559	20.4	11.84
47.02	3	60	3.521	559	21.4	8.05
47.03	3	80	4.695	559	22.0	5.70
47.04	3	40	2.348	541	60.0	11.42
47.05	3	60	3.521	538	59.8	7.87
47.06	3	80	4.695	537	60.6	5.13
47.07	3	60	3.521	541	74.6	7.53
47.08	3	80	4.695	540	74.6	5.98(?)
47.09	3	100	5.869	540	75.0	5.71(?)

x) type of blockage 1: 15 % central, symmetrical blockage (see Fig. 2)
2: 41 % central, symmetrical blockage (see Fig. 2)
3: 47 % edge blockage (see Fig. 3)

Table 2: Measured difference between local coolant temperature and inlet temperature, $\Delta\vartheta$, Exp. No. 15.01

z mm	i,j -	$\Delta\vartheta$ °C	z mm	i,j -	$\Delta\vartheta$ °C
10	5,2	13.74	60	2,2	9.81
10	6,2	14.66	60	3,2	8.76
10	5,3	12.13	60	4,2	8.72
			60	5,3	7.29
20	2,2	13.12			
20	3,2	11.23	80	2,2	11.74
20	5,2	11.31	80	3,2	9.62
20	6,2	10.84	80	4,2	8.76
20	5,3	12.12	80	5,2	7.38
40	2,2	12.33	100	2,2	10.77
40	3,2	9.73	100	3,2	8.55
40	4,2	9.21	100	4,2	7.94
40	5,2	8.55	100	5,2	6.69
40	6,2	7.30	100	6,2	5.44
40	5,3	8.83			

z: Axial distance downstream of the blockage

i,j: Subchannel location (see Fig. 2)

Table 3: Measured difference between local coolant temperature and inlet temperature, $\Delta\vartheta$, Exp. No. 15.10

z mm	i,j -	$\Delta\vartheta$ °C	z mm	i,j -	$\Delta\vartheta$ °C
10	5,2	5.24	60	2,2	4.10
10	6,2	6.22	60	3,2	3.69
10	5,3	5.77	60	4,2	3.82
			60	5,3	3.59
20	2,2	5.34			
20	3,2	5.08	80	2,2	4.72
20	5,2	5.65	80	3,2	3.69
20	6,2	5.06	80	4,2	3.50
20	5,3	6.03	80	5,2	3.09
40	2,2	4.49	100	2,2	4.43
40	3,2	4.27	100	3,2	3.72
40	4,2	4.19	100	4,2	3.17
40	5,2	4.13	100	5,2	2.79
40	6,2	3.73	100	6,2	2.32
40	5,3	3.67			

For explanation of symbols see Table 2

Table 4: Measured difference between local coolant temperature and inlet temperature, $\Delta\vartheta$, Exp. No. 41.01

z mm	i,j -	$\Delta\vartheta$ °C
10	2,2	17.28
	3,2	17.19
	4,2	19.56
	5,2	16.27
	6,2	15.90
	7,2	19.24
	8,2	19.79
	9,2	19.92
	10,2	20.55
	11,2	11.37
	12,2	7.09
	5,3	18.70
	7,3	18.64
	8,3	18.26
	9,4	4.81
10	10,4	9.53
20	3,2	19.80
20	5,2	16.80
20	5,3	18.32
20	8,4	11.42
20	9,4	6.22
40	3,2	16.11
40	4,2	15.48
40	5,3	15.56
40	8,4	12.29
40	9,4	9.16
40	10,4	7.09
60	2,2	18.23
	3,2	16.11
	4,2	14.80
	5,2	*
	6,2	13.32
	5,3	14.25
	8,4	11.52
	9,4	9.50
60	10,4	8.82
80	2,2	18.50
80	4,2	15,24
80	5,2	14,31
80	5,3	13,66
100	2,2	18.14
100	3,2	15.07
100	4,2	15.36
100	5,3	13.05
125	2,2	18.67
150	2,2	18.55
175	2,2	17.97

For explanation of symbols see Table 2

* thermocouple failed with this experiment

Table 5: Measured difference between local coolant temperature and inlet temperature, $\Delta\vartheta$, Exp. No. 41.06

z mm	i,j -	$\Delta\vartheta$ °C	z mm	i,j -	$\Delta\vartheta$ °C
10	2,2	9.08	60	2,2	8.90
	3,2	9.10		3,2	8.47
	4,2	10.35		4,2	7.98
	5,2	9.52		5,2	8.10
	6,2	9.55		6,2	7.97
	7,2	10.11		5,3	7.58
	8,2	10.61		8,4	7.18
	9,2	10.60		9,4	5.67
	10,2	10.86	60	10,4	4.85
	11,2	7.62			
	12,2	4.19	80	2,2	8.09
	5,3	9.77	80	4,2	7.36
	7,3	10.38	80	5,2	7.15
	8,3	10.25	80	5,3	7.12
	9,4	4.02			
10	10,4	7.60	100	2,2	8.54
			100	3,2	7.67
			100	4,2	7.47
20	3,2	10.12	100	5,3	6.88
20	5,2	8.97			
20	5,3	9.73	125	2,2	8.84
20	8,4	6.08			
20	9,4	3.55	150	2,2	7.99
40	3,2	8.70	175	2,2	7.22
40	4,2	8.39			
40	5,3	9.03			
40	8,4	7.62			
40	9,4	5.04			
40	10,4	4.84			

For explanation of symbols see Table 2

Table 6: Measured difference between local coolant temperature and inlet temperature, $\Delta\vartheta$, Exp. No. 47.01

z mm	i,j -	$\Delta\vartheta$ °C	z mm	i,j -	$\Delta\vartheta$ °C
10	2,2	23.25	40	4,2	24.29
	3,2	17.66	40	5,2	22.27
	7,2	18.51	40	6,2	26.35
	8,2	20.52	40	20,2	16.21
	9,2	18.70			
	11,2	18.66	60	3,2	23.92
	12,2	19.70	60	4,2	22.94
	13,2	20.78	60	5,2	20.40
	15,2	23.80			
	16,2	29.09	80	4,2	20.67
	17,2	24.00	80	5,2	19.71
	19,2	34.31	80	6,2	18.91
	20,2	31.80			
	21,2	32.42	100	2,2	22.59
	23,2	11.17	100	3,2	22.07
	24,2	5.92	100	4,2	19.50
10	25,2	2.87	100	18,2	9.93
20	5,2	27.52	150	4,2	19.41
20	6,2	29.83			
20	7,2	29.44	200	3,2	21.42
20	17,2	33.17			
20	18,2	33.66	250	4,2	21.52

z: Axial distance downstream of the blockage

i,j: Subchannel location (see Fig. 3)

Table 7: Measured difference between local coolant temperature and inlet temperature, $\Delta\vartheta$, Exp. No. 47.06

z mm	i,j -	$\Delta\vartheta$ °C	z mm	i,j -	$\Delta\vartheta$ °C
10	2,2	11.21	40	4,2	12.54
	3,2	12.06	40	5,2	12.33
	7,2	7.60	40	6,2	12.83
	8,9	8.46	40	20,2	11.75
	9,2	8.37			
	11,2	9.19	60	3,2	12.04
	12,2	9.12	60	4,2	12.07
	13,2	9.46	60	5,2	11.68
	15,2	9.68			
	16,2	9.93	80	4,2	11.79
	17,2	9.67	80	5,2	11.83
	19,2	11.52	80	6,2	11.74
	20,2	9.82			
	21,2	11.74	100	2,2	10.60
	23,2	5.46	100	3,2	10.75
	24,2	2.78	100	4,2	10.64
10	25,2	1.03	100	18,2	6.78
20	5,2	13.22	150	4,2	9.24
20	6,2	14.58			
20	7,2	*	200	3,2	9.35
20	17,2	14.72			
20	18,2	15.19	250	4,2	9.93

For explanation of symbols see Table 6

* thermocouple failed with this experiment

Table 8: Variation of Axial Mesh Size in the Wake Region for the SABRE Calculation of Exp. No. 15.04

z mm	i,j -	$\Delta\vartheta$ °C measured	calculated 10	calculated 5	calculated 2.5 mm	axial mesh size
10	5,2	12.80	11.8	12.7	11.3	
10	6,2	14.20	13.0	14.0	12.4	
10	5,3	13.00	13.1	13.7	12.1	
20	2,2	13.21	10.3	10.5	9.3	
20	3,2	11.16	10.1	10.6	9.5	
20	5,2	11.65	11.4	12.9	11.9	
20	6,2	10.62	9.5	11.8	11.3	
20	5,3	12.33	12.1	14.1	12.6	
40	2,2	11.63	9.4	9.7	8.8	
40	3,2	9.48	8.6	9.2	8.4	
40	4,2	8.96	8.2	9.1	8.3	
40	5,2	8.38	7.5	8.4	7.8	
40	6,2	7.18	5.8	6.5	6.0	
40	5,3	8.44	7.1	8.1	7.3	
60	2,2	9.47	8.9	9.1	8.5	
60	3,2	8.53	7.8	8.0	7.4	
60	4,2	8.63	7.1	7.3	6.7	
60	5,3	7.21	5.8	5.9	5.3	
80	2,2	11.12	9.5	9.4	8.5	
80	3,2	9.64	7.9	7.9	7.1	
80	4,2	8.38	7.0	7.0	6.3	
80	5,2	7.08	5.9	5.8	5.3	
100	2,2	10.61	9.9	9.8	8.6	
100	3,2	8.44	8.2	8.1	7.2	
100	4,2	7.47	7.2	7.1	6.3	
100	5,2	6.38	5.9	5.8	5.3	
100	6,2	5.16	4.8	4.7	4.4	
	sum of mass sources:		5.8	15	86	x 10^{-4}
	computing time (CPU):		10	10	10	min

For explanation of symbols see Table 2

Table 9: Results of SABRE Calculation of Exp.s No. 15.01 and 15.10

z	i,j	$\Delta\vartheta$ (calculated) °C		
mm	-	15.01	15.10	
10	5,2	11.9	5.4	
10	6,2	12.9	5.9	
10	5,3	13.1	5.8	
20	2,2	9.7	4.5	
20	3,2	9.7	4.5	
20	5,2	11.6	5.4	
20	6,2	9.5	5.5	
20	5,3	12.1	5.9	
40	2,2	8.9	4.2	
40	3,2	8.1	4.0	
40	4,2	7.7	4.0	
40	5,2	7.1	3.9	
40	6,2	5.4	3.1	
40	5,3	6.6	3.8	
60	2,2	8.5	3.9	
60	3,2	7.4	3.4	
60	4,2	6.7	3.2	
60	5,3	5.2	2.6	
80	2,2	8.8	3.9	
80	3,2	7.4	3.3	
80	4,2	6.5	3.0	
80	5,2	5.4	2.5	
100	2,2	9.2	4.1	
100	3,2	7.6	3.4	
100	4,2	6.6	3.0	
100	5,2	5.5	2.5	
100	6,2	4.5	2.0	
	sum of mass sources:	12	22	x 10^{-4}
	computing time (CPU):	10	10	min

For explanation of symbols see Table 2

Table 10: Results of SABRE Calculation of Exp. No. 41.01

z mm	i,j -	$\Delta\vartheta$ (calculated) °C	z mm	i,j -	$\Delta\vartheta$ (calculated) °C
10	2,2	16.5	60	2,2	14.7
|	3,2	16.3	|	3,2	14.0
|	4,2	16.4	|	4,2	14.2
|	5,2	16.6	|	5,2	15.0
|	6,2	17.2	|	6,2	16.0
|	7,2	17.7	|	5,3	16.3
|	8,2	18.4	|	8,4	13.3
|	9,2	19.1	|	9,4	6.1
|	10,2	17.5	60	10,4	3.2
|	11,2	2.7			
|	12,2	2.1	80	2,2	14.2
|	5,3	17.1	80	4,2	13.0
|	7,3	18.1	80	5,2	12.9
|	8,3	18.7	80	5,3	13.0
|	9,4	5.6			
10	10,4	2.6	100	2,2	13.9
			100	3,2	12.6
20	3,2	15.6	100	4,2	12.0
20	5,2	16.3	100	5,3	11.0
20	5,3	17.4			
20	8,4	19.9	125	2,2	13.8
20	9,4	7.1			
			150	2,2	14.3
40	3,2	14.7			
40	4,2	14.9	180	2,2	14.8
40	5,3	18.3			
40	8,4	20.1			
40	9,4	7.5			
40	10,4	3.1			

sum of mass sources: $6.5 \cdot 10^{-4}$

computing time (CPU): 30 min

For explanation of symbols see Table 2

Table 11: Results of SABRE Calculation of Exp. No. 47.01

z mm	i,j -	$\Delta\vartheta$ (calculated) °C	z mm	i,j -	$\Delta\vartheta$ (calculated) °C
10	2,2	23.8	40	4,2	20.6
|	3,2	21.6	40	5,2	19.8
|	7,2	21.6	40	6,2	19.8
|	8,2	21.9	40	20,2	19.7
|	9,2	22.4			
|	11,2	23.3	60	3,2	18.4
|	12,2	23.7	60	4,2	20.0
|	13,2	24.1	60	5,2	19.1
|	15,2	24.9			
|	16,2	25.3	80	4,2	19.6
|	17,2	25.8	80	5,2	18.4
|	19,2	27.1	80	6,2	18.2
|	20,2	27.9			
|	21,2	28.8	100	2,2	18.1
|	23,2	2.5	100	3,2	16.3
|	24,2	2.1	100	4,2	19.3
10	25,2	1.9	100	18,2	8.9
20	5,2	20.7	150	4,2	18.6
20	6,2	20.7			
20	7,2	21.0	200	3,2	16.1
20	17,2	26.8			
20	18,2	27.3	250	4,2	17.5

sum of mass sources: $1.2 \cdot 10^{-2}$

calculating time (CPU): 160 min

For explanation of symbols see Table 6

Table 12: Variation of some Important Calculational Parameters for the SABRE Calculation of Exp. No. 15.01

z	i,j	$\Delta\vartheta$ (calculated) °C						
mm	-	nominal	Γ_H = 0.0	Γ_H = 0.1	axial friction f. halved/doubled		all fricton f.s halved/doubled	
10	5,2	11.9	11.9	11.9	13.2	9.4	13.0	9.4
10	6,2	12.9	12.8	12.5	14.2	8.0	13.9	7.6
10	5,3	13.1	13.0	13.0	14.0	9.8	13.7	9.2
20	2,2	9.7	9.7	9.7	11.1	7.8	10.7	7.8
20	3,2	9.7	9.7	9.7	11.2	7.5	11.1	7.3
20	5,2	11.6	11.5	11.5	13.7	7.0	13.6	6.8
20	6,2	9.5	9.4	9.5	14.2	5.4	13.9	5.3
20	5,3	12.1	12.0	12.0	14.5	6.5	14.3	6.2
40	2,2	8.9	8.8	8.8	10.6	6.8	10.4	6.8
40	3,2	8.1	8.1	8.1	10.1	6.1	10.0	6.1
40	4,2	7.7	7.6	7.7	10.3	5.6	10.1	5.5
40	5,2	7.1	7.0	7.0	10.2	4.8	10.0	4.7
40	6,2	5.4	5.3	5.3	8.2	3.8	8.2	3.8
40	5,3	6.6	6.5	6.5	10.2	4.3	10.0	4.2
60	2,2	8.5	8.4	8.5	10.1	7.0	10.1	7.1
60	3,2	7.4	7.3	7.3	8.9	6.0	8.8	6.0
60	4,2	6.7	6.6	6.6	8.2	5.3	8.2	5.3
60	5,3	5.2	5.1	5.2	6.9	4.0	6.9	4.0
80	2,2	8.8	8.7	8.8	10.1	7.3	10.1	7.3
80	3,2	7.4	7.3	7.3	8.6	6.1	8.5	6.1
80	4,2	6.5	6.4	6.5	7.7	5.4	7.7	5.4
80	5,2	5.4	5.3	5.4	6.5	4.5	6.5	4.5
100	2,2	9.2	9.1	9.2	10.6	7.7	10.4	7.7
100	3,2	7.6	7.5	7.6	8.7	6.4	8.6	6.4
100	4,2	6.6	6.6	6.6	7.6	5.6	7.6	5.7
100	5,2	5.5	5.4	5.5	6.4	4.8	6.3	4.8
100	6,2	4.5	4.5	4.5	5.1	4.1	5.1	4.2
sum of mass sources:		12	5	5	160	120	260	110 x 10^{-4}
computing time (CPU):		10	5	5	5	5	5	5 min

For explanation of symbols see Table 2

Γ_H: Total (molecular and turbulent) thermal diffusivity

APPENDIX

AN OUTLINE OF THE THEORY AND NUMERICAL REPRESENTATION

A1 Purpose

The object of this appendix is to give a brief outline of the numerical methods used in SABRE, and to detail precisely the assumptions made to simplify the problem and to procure convergence of the solution procedure. Details are also given of the empirical relations used for friction and diffusivity.

A2 Definition of the Problem

The dependent variables of the problem are the values of pressure p, enthalpy, h (or temperature, t), and velocity, components u, v, and w, at each of their respective nodes throughout the calculational zone. These quantities have already been defined with their relations with the control volumes in Section 3.2. Thus defined the velocities determine the momentum transport per unit mass, and the enthalpies the heat transport per unit mass across the faces of the control volumes. The velocities are also used directly in the empirical relations for frictional resistance and heat transfer. A further point to note is that the properties of fluid entering a control volume are assumed to be those of the control volume upstream in the appropriate direction. This upwind, or donor cell diferencing procedure is in accord with physical intuition, and is also necessary for the convergence of the solution procedure. It is employed for both the heat and momentum fluxes.

A3 Simplifying Assumptions

The Subchannel Approximation

The momentum equations for a continuum contain terms expressing the transport of each momentum component across each face of the control volume. Two different classes of term have been neglected in this analysis. The first is the so-called 'normal stress' terms which represent the diffusion of, for example, z directed momentum in the z direction, etc. This neglect is justified because wall friction is the dominant force, because of the presence of the rods.

The second set of terms which have been omitted from the equations comprises those representing the convection of x-directed momentum in the y direction and y-directed momentum in the x direction. This allows the use of a simpler solution procedure in both square and triangular cases, and avoids the need for resolution of the transverse velocities, which is acutely embarrassing in the triangular case where successive u velocities are inclined at 60 degrees to each other. This 'subchannel approximation' is justified if the spacing of the rods forming the subchannels is sufficiently small relative to their diameter, because the respective momenta will be destroyed in the contraction and expansion of the flow path between subchannels. In a sense the terms are implicitly included, because the destruction of the momentum produces an increase in pressure, in the empirical correlations for the cross flow friction. Although such terms could, at the cost of extra computing time be included in the square mesh version, their incorporation in the triangular mesh involves gross difficulties

of resolution of velocities because of the above-mentioned non-alignment. Moreover, in both cases their formulation in the SABRE problem is difficult, because of the shape of the passages between the rods. The convection of x and y directed momenta over the axial (z) faces of the control volumes meets no such physical obstacles and is explicitly represented, as is the transport of x, y, and z directed momentum in each respective direction.

A4 Empirical Correlations

The friction factor formulae used in the momentum equations take different forms according to the flow régime in the control volume being considered. At this stage of development of SABRE two régimes have been identified for the axial (z direction) friction factors, and three for the transverse (or crossflow) friction factors.

A4.1 Axial Friction Factors

The two cases considered are laminar and turbulent flow. There is no changeover point, the laminar to turbulent transition is represented by adding the two expressions. This technique gives as good a formulation as any available in the transition region, and has the advantage, for the solution procedure, of being continuous in magnitude and slope with respect to velocity. The two formulae are:-

1 (Laminar flow (17)

$$f_z^l = 8 \; / \; Re_w$$

2 Turbulent flow. This is the well known formulation of Blasius for pipe flow. It is adapted to the subchannel situation by the use of the hydraulic diameter concept.

$$f_z^t = 0.024 \; Re_w^{-0.2}$$

The total axial friction is then:-

$$f_z = f_z^l + f_z^t$$

where:- $Re_w = D_h \rho |w| \mu$

and $D_h = 4 \; A_w / P_w$ = Hydraulic diameter of the section of subchannel

A_w = Flow area of subchannel for w velocity

P_w = Wetted perimeter of the section

ρ = Density in the control volume

$|w|$ = Magnitude of axial velocity

μ = Viscosity

A4.2 Cross Flow Friction Factors

These are the same for the x and y velocities, but three flow regimes are distinguished. The cases are laminar and turbulent cross flow, and the case where the cross flow is small and the regime would be laminar but for turbulence generated by strong axial flow. This case is called oblique flow. For the transverse direction the friction factor chosen is the largest of the three values, and the discontinuities introduced by this choice do not upset the solution procedure. For the sake of example the u velocity has been used in the definitions.

1 Laminar flow using an 'equivalent' parallel - sided channel in fully developed flow.

$$f_c^l = 3\left(\frac{H_{xy}}{H}\right)^2 \left(\frac{\rho u H_{xy}}{\mu}\right)^{-1}$$

2 Turbulent flow due to McAdams (16)

$$f_c^t = 0.2 \left(\frac{H_{xy}}{p}\right) \left(\frac{\rho u H_{xy}}{\mu}\right)^{-1}$$

3 Oblique flow based on a Couette - flow analysis of the above equivalent channel in fully developed turbulent flow.

$$f_c^o = 3 \left(\frac{H_{xy}}{H}\right)^2 \left[\frac{u H_{xy}}{\mu_{eff}} \left(1.0 + 2.16 \frac{D_h}{H_{xy}}\right)\right]^{-1}$$

$$f_c = \text{Max}\ (f_c^l,\ f_c^t,\ f_c^o)$$

Where the new symbols are:-

H_{xy} = gap between pins

H = an equivalent gap = $H_{xy} + \frac{D}{2}(1 - \sqrt{3}/2)$

D = pin diameter

P = pin pitch

μ_{eff} = effective viscosity, defined in the next Section A4.3

A4.3 Effective Viscosity and Thermal Diffusivity

The effective viscosity is assumed to be the sum of the dynamic viscosity and a turbulent contribution thus:-

$$\mu_{eff} = \mu + \mu_t$$

and

$$\mu_t = 0.03\ \rho\, \text{Max}\ (u,v,w)\ D_h\ (f_z)^{\frac{1}{2}}$$

The use of Max (u,v,w) is a first attempt to allow for the generation of turbulence by fluid motion whatever its direction.

Similarly the effective thermal exchange coefficient is the sum of a turbulent and a laminar component. Thus, in terms of viscosities and Prandtl numbers (σ) the effective exchange coefficient is:-

$$\Gamma_{eff} = \frac{\mu}{\sigma} + \frac{\mu_t}{\sigma_t}$$

The turbulent Prandtl number, σ_t used is as proposed by Nijsing and Eifler (17).

A5 The Finite Difference Equations Embodied in the SABRE Program

The equations to be solved are those representing the conservation of momentum, mass, and enthalpy. The principal dependent variables are the velocity components u, v, and w, the static pressure , and the enthalpy h, (or temperature t, which is related to enthalpy) at each node in the zone of calculation. For a chosen node p the equations of conservation of each momentum component take, after manipulation into the form required by the SIMPLE algorithm, the following form:-

$$\phi_p \sum_n A_n^\phi = \sum_n A_n^\phi \phi_n + B_p^\phi + \bar{a} (P_{p-1} - P_p) \qquad \ldots \quad 1$$

where: the sum is over the six neighbours n

B_P^ϕ is the source of momentum in the cell

$\bar{a} (P_{p-1} - P_p)$ is the net force acting on the cell in the direction of the component ϕ_p which may be u, v, or w.

The coefficients A_n^ϕ are combined convection and diffusion coefficients defined in a way which includes the upwind or donor cell differencing procedure or the central difference procedure according to the relative importance of convective and diffusion fluxes. To illustrate this we will examine the coefficient in the w velocity equation on the x+ face of the cell. Then:-

$$A_{x+}^W = T^*_{x+} - L_{x+}$$

$$T^*_{x+} = \tfrac{1}{2} \{T_{x+} + |L_{x+}| + |(T_{x+} - |L_{x+}|)|\}$$

$$L_{x+} = \tfrac{1}{2} \dot{m}''_{x+} a_{x+}$$

$$T_{x+} = \mu_{eff} a_{x+}/\delta_{x+} \qquad (a = \text{area}, \delta = \text{mesh spacing})$$

The enthalpy equation is of the same form but without the pressure gradient term.

The source term $B_p^\phi = S_u^\phi + S_p^\phi \phi_p$

Where S_u and S_p depend on the resistance laws (S is subtracted from the coefficient of ϕ_p in equation 1 above in order to increase diagonal dominance).

Thus we have a set of equations for four of the five principal dependant variables. For the fifth, the pressure, there remains only the mass continuity equation, which written simply is:-

$$\text{div } (G) = 0$$

In the SABRE finite difference form this becomes:-

$$\sum_n \bar{\rho}_n a_n \phi_n = 0$$

where n is the six faces of the cell

$\bar{\rho}_n$ is the density on face n which has area a_n

ϕ_n is the velocity normal to face n

But this equation does not explicitly contain the pressure. One of the key features of the SIMPLE algorithm will now be introduced. This is the use of an equation which gives not the pressure directly, but the correction P' to an assumed or previously calculated pressure P. This equation is of the same form as the other four basic equations and can therefore be treated in the same way. Its derivation is founded on two principles.

1 There exists a relation between the pressure corrections P'_p and a resultant correction to each velocity ϕ_p and this relation is approximately

$$\phi'_p = D_p^\phi (P'_{p\_} - P'_p)$$

where the D term is a known function of the coefficients in the momentum equations.

2 The approximation is sufficiently good to allow convergence on to the correct solution of the equations and its approximate nature is without influence on this solution. This is because if the solution is correct the pressure corrections will all be zero.

From these premises we arrive at an equation of the same form as the velocity and enthalpy equations, but the source term B now represents the so-called mass source, which is the local departure from satisfaction of the mass continuity equation. Thus, summing as usual over the six neighbours n.

$$P'_p \sum_n A^p_n = \sum_n A^p_n P'_n + B^p_p$$

in which for example

$$A^p_{x-} = \bar{\rho}_{x-} a_{x-} D^u_p$$

$D^u_p = a_x / A^u_p$ and A^u_p is identical to the A^u_p in the momentum eqn.

There exist appropriate specifications of the A coefficients and source terms to satisfy any self-consistent choice of internal or external boundary conditions for a physical problem. With one exceptional case, the reader is referred to the program manual (15). The exception which will now be described is the technique used for passing from the equations for the square array to the triangular. Here advantage is taken of the fact that a triangular array is topologically similar to a square array with every alternate passage in one transverse direction blocked. The equations are still valid provided the subchannel approximation of Section A3 is valid. The breakage of the links is accomplished by setting to zero the appropriate flow areas and altering the source terms in the equation set. The modified terms are:-

$S_u = 0$

S_p = some large negative number eg -10^{20}

A6 The Solution Procedure

The starting point is a set of guessed fields of velocities, enthalpies and pressures. These may be quite arbitrary and are without influence on the final solution, but the better the starting point, the quicker the procedure converges on the final correct solution. For example an often used, convenient and effective starting point, even for problems with large recirculating zones is:-

all u = v = 0

all w = constant = inlet values

all t(h) = constant

P constant across the section, with uniform gradient in the axial direction.

The solution procedure is most easily described by a flow diagram, Figure 9. As each variable is calculated, all the others are assumed fixed at their latest known values. This is another way of saying that the procedure decouples the five simultaneous equation sets, allowing sequential solution. The coupling is then introduced at the stage of the application of the pressure corrections and associated velocity corrections.

There is, however, a number of special practices designed to procure rapid and effective convergence of the overall procedure. Because of the decoupling of the equations, different numerical techniques may be employed for different equations. The methods are therefore chosen according to the different forms of the particular equations for the various variables.

1 For the transverse (ie u and v) velocities the equations are reduced by the subchannel approximation to the form:-

$$d_k \phi_k = a_k \phi_{k+1} + c_k$$

with each velocity depending only on the neighbouring values in the axial direction. The set of equations may be expressed in a form which is solved by the inversion of a tri-diagonal matrix. This is a particularly simple form of matrix to invert. The algorithm used is a forward elimination/backward substitution technique known in SABRE as the T D M A (Tri-Diagonal Matrix Algorithm)

2 The other three equations, in w, p', and h take the general form with all six neighbours n included:-

$$A_{ijk}\, \phi_{ijk} = \sum_n' A^n_{ijk}\, \phi^n + B_{ijk}$$

The presence of the six neighbours makes direct matrix inversion much more difficult, for now access to the whole three dimensional field of coefficients is needed and this is too expensive in computer storage. The co-ordinate directions are therefore treated successively in an iterative scheme. This is accomplished by temporarily shifting four of the six neighbours into the source term B. Thus, for w velocity and calculating along the x direction we now have:-

$$A_{ijk}\, w_{ijk} = A^{x+}_{ijk}\, w_{i+1,jk} + A^{x-}_{ijk}\, w_{i-1,jk} + B'_{ijk}$$

which is amenable to inversion by TDMA. The same process is then applied to the y direction for the same k plane. The interaction between successive k planes could be taken into account by a similar sweep in the axial direction, but this again is too costly, for the same reason as for the direct inversion. The above method is therefore used in each plane in turn, and the plane to plane interactions are subsequently taken into account by applying a block adjustment, uniform in each plane, but differing from plane to plane. This adjustment is calculated in conformity with overall mass continuity, and with the boundary conditions. The result is an iterative process which requires a few applications (typically 2 for w and h, and 6 for pressure) per cycle of the SIMPLE procedure.

A7 Special Measures to Facilitate Convergence

There are two measures which have to be taken to improve the convergence of SIMPLE in SABRE. One is the well known and simple process of under-relaxation, which is needed for both pressure and velocity corrections. It is applied thus:-

to the pressure correction;

$$P_p = P_p^* + r_p P_p'$$

in the correction of the velocities;

$$\phi_p = r_v \phi_u + (1-r_v) \phi_o$$

where: r_p and r_v are respectively the pressure and velocity under-relaxation parameters, ϕ_u is the corrected velocity without under-relaxation, and ϕ_o is the velocity before application of any correction.

The second measure is more subtle and is required because there may arise, particularly in the early stages of a calculation, cells with outflow over all six faces. In this case there is no upstream point from wich to execute the differencing procedure, which therefore breaks down. The effect of this breakdown is removed by the addition to the momentum and enthalpy equations of a false source, given (for example) for the w velocity equation by:-

$$-(w_p - w_p^*) \quad \langle \text{div } (G) \rangle$$

here $w_p - w_p^*$ is the change in w from one cycle to the next

and $\langle \text{div } (G) \rangle = \text{div } (G)$ if div $(G) > 0$

$= 0$ if div $(G) \leqslant 0$

This ensures that the sum A_s of the coefficients in the equations can never be negative and thereby removes the instability. It is without influence on the final solution for which both $(w_p - w_p^*)$ and div (G) are zero.

A similar adjustment is made to the transverse velocity equations, with a simplified form of div (G) because of the subchannel approximation.

A8 Convergence Criterion

The 'mass source' mentioned in Section A5 provides a convenient quantity which is directly related to the degree of non-satisfaction of the equations. In practice it is necessary to examine the maximum mass source and the sum of the absolute values of the mass sources to ensure convergence. The criterion adopted is that the sum of the sources must be less than a prescribed fraction of the total mass of fluid in the calculational domain, and the maximum mass source must be small enough relative to the mass in a control volume.

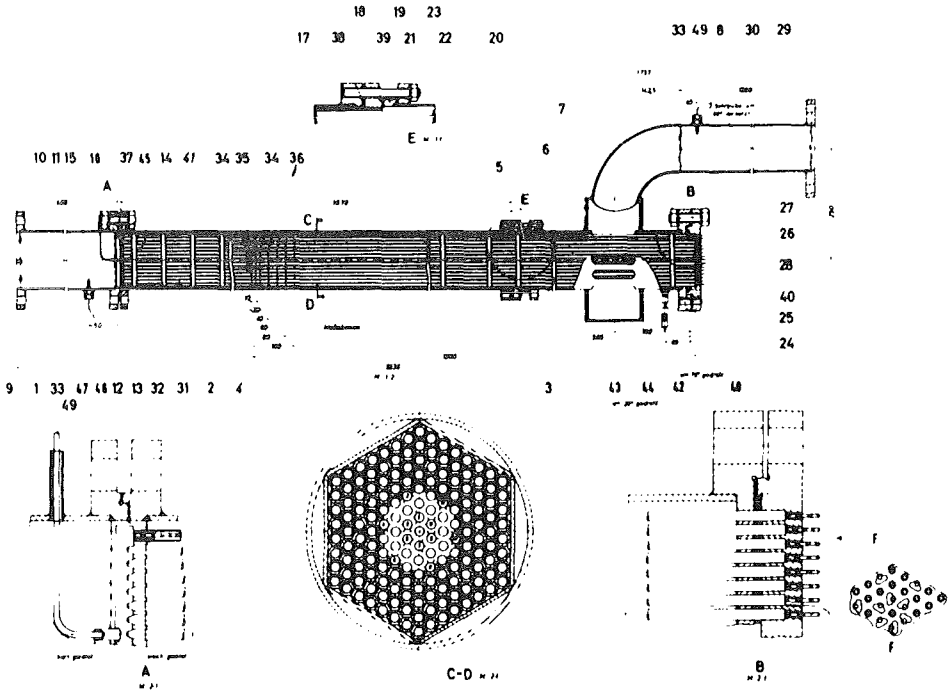

Fig. 1 Test Section for the Measurement of Temperature Distributions

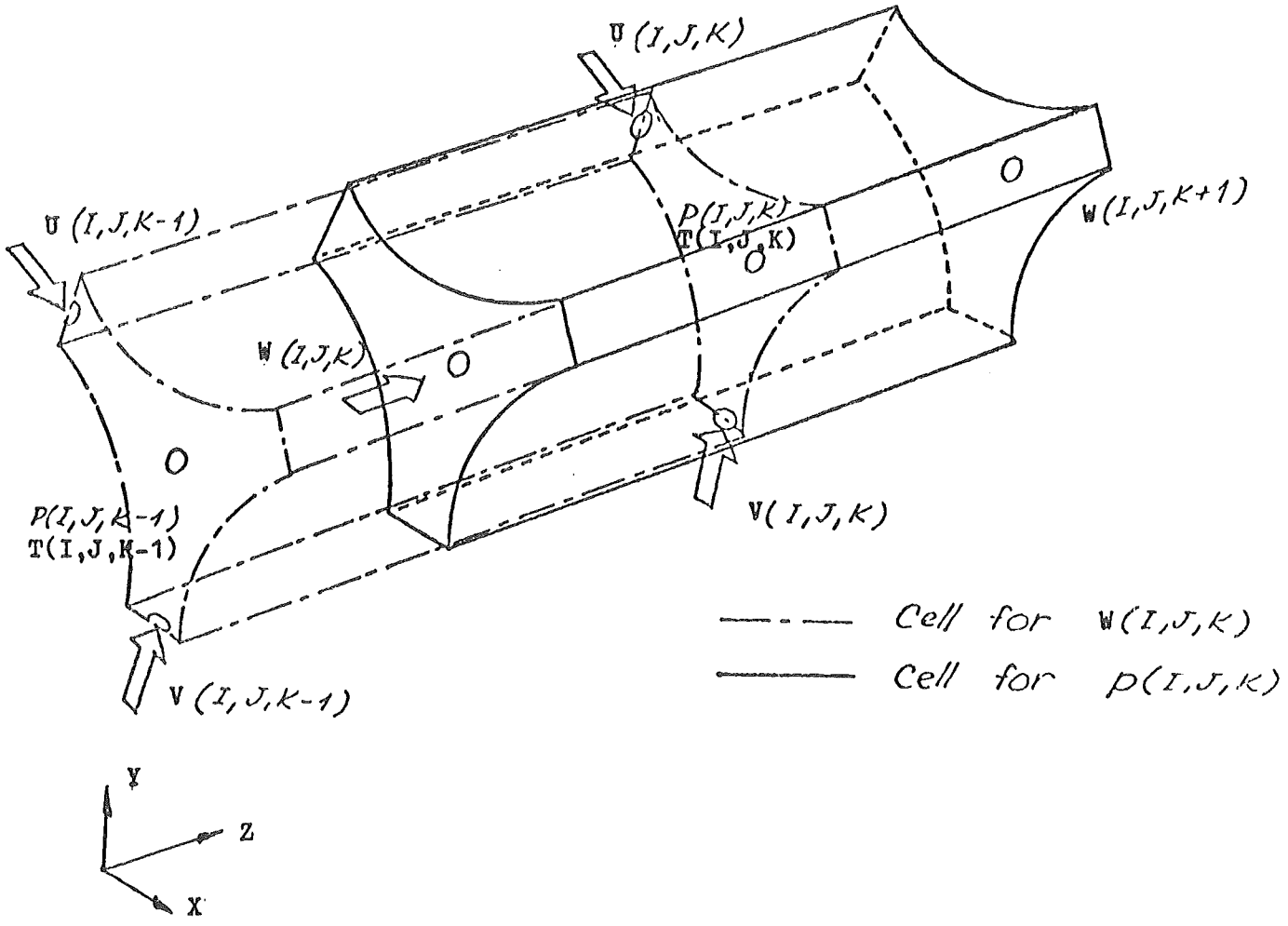

FIGURE 2: ISOMETRIC VIEW OF W AND P CELLS AND SURROUNDING VELOCITY NODES

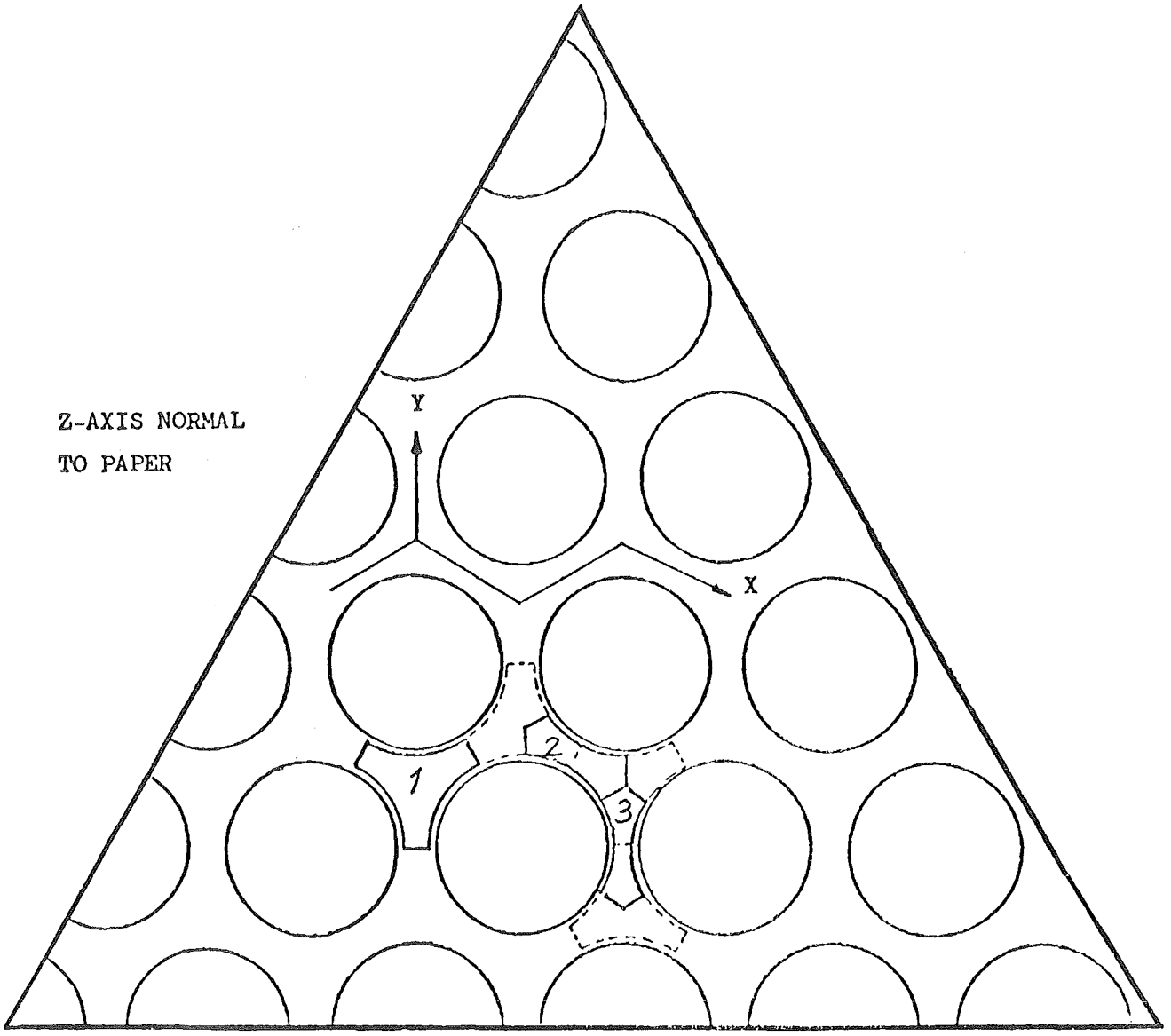

1 denotes control volume for Z-momemtum equation

2 denotes control volume for X-momentum equation

3 denotes control volume for Y-momentum equation

FIGURE 3: AXES AND SUBCHANNELS

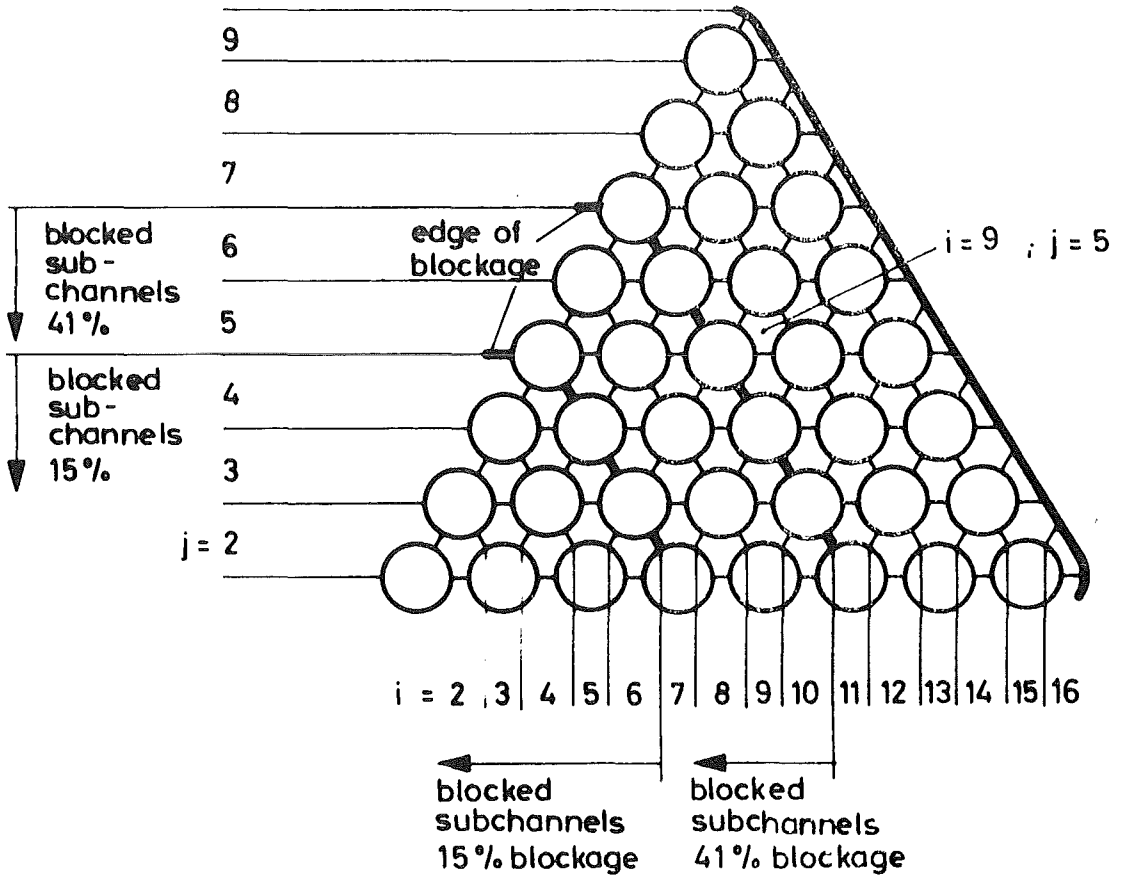

Fig. 4 Rod, Subchannel and Blockage Arrangement for SABRE Calculations
15 % and 41 % central, symmetrical blockage.

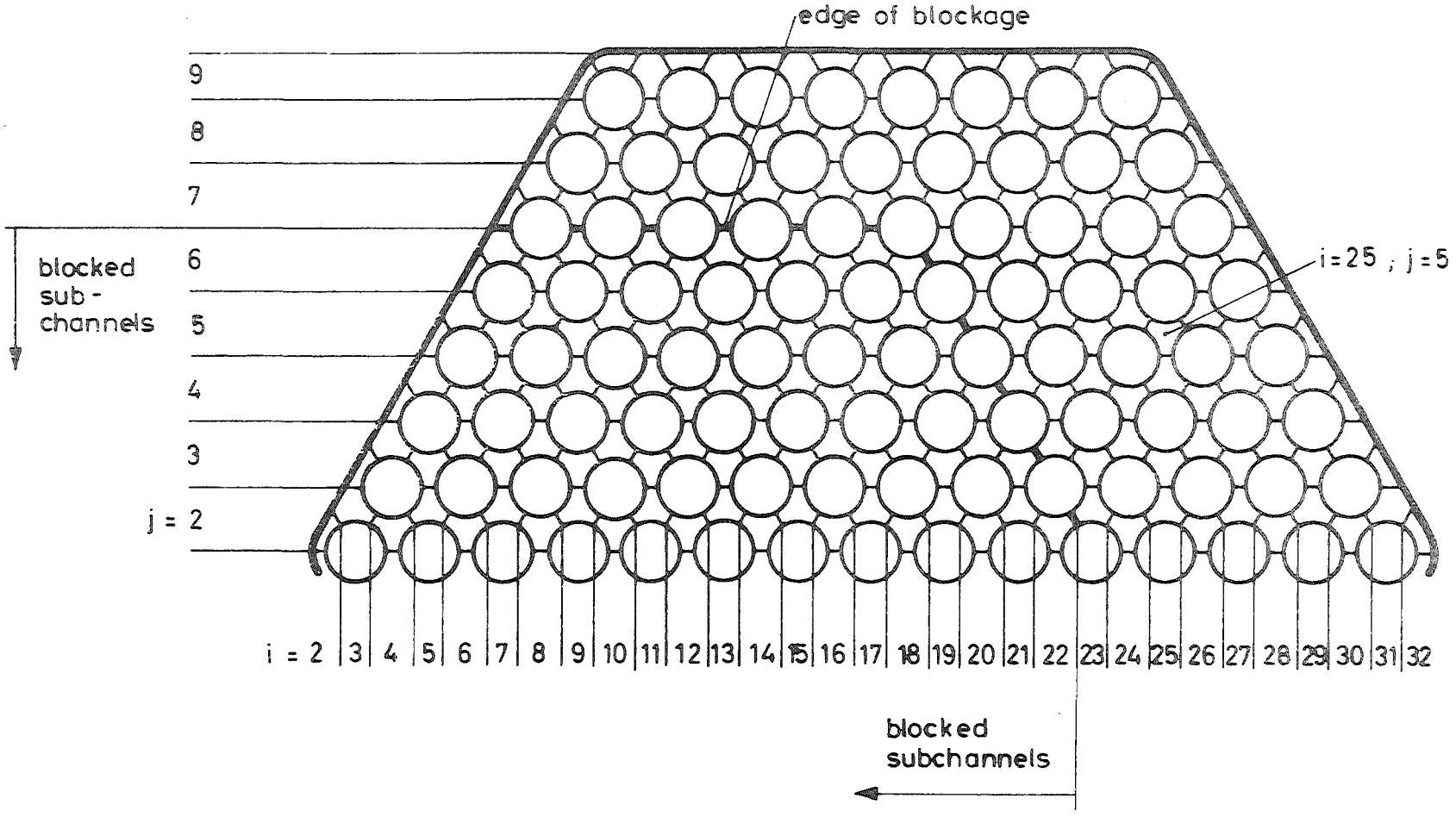

Fig. 5 Rod Subchannel and Blockage Arrangement for SABRE Calculations 47% edge blockage.

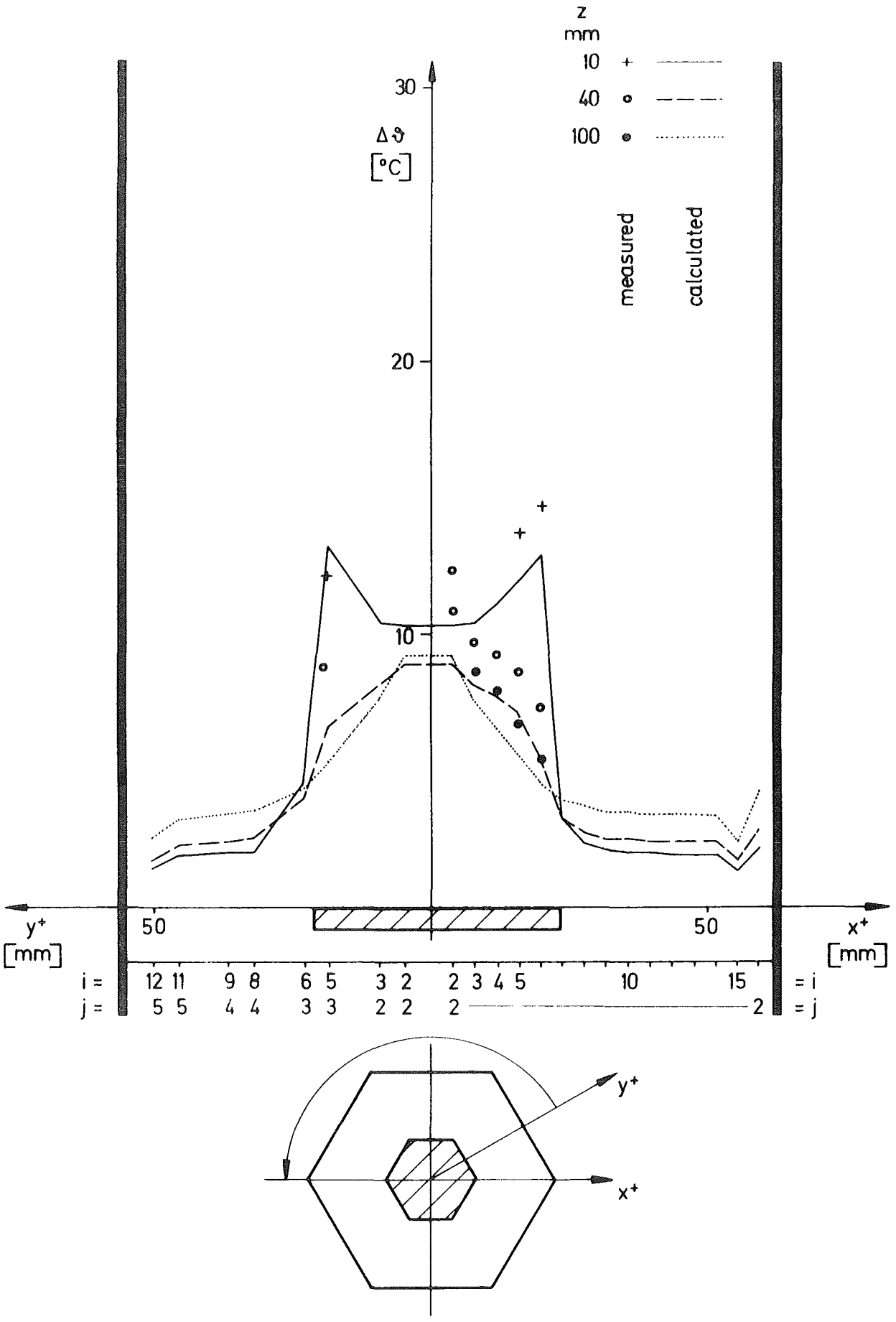

Fig. 6 Comparison of measured and calculated temperature differences for Exp. No. 15.01

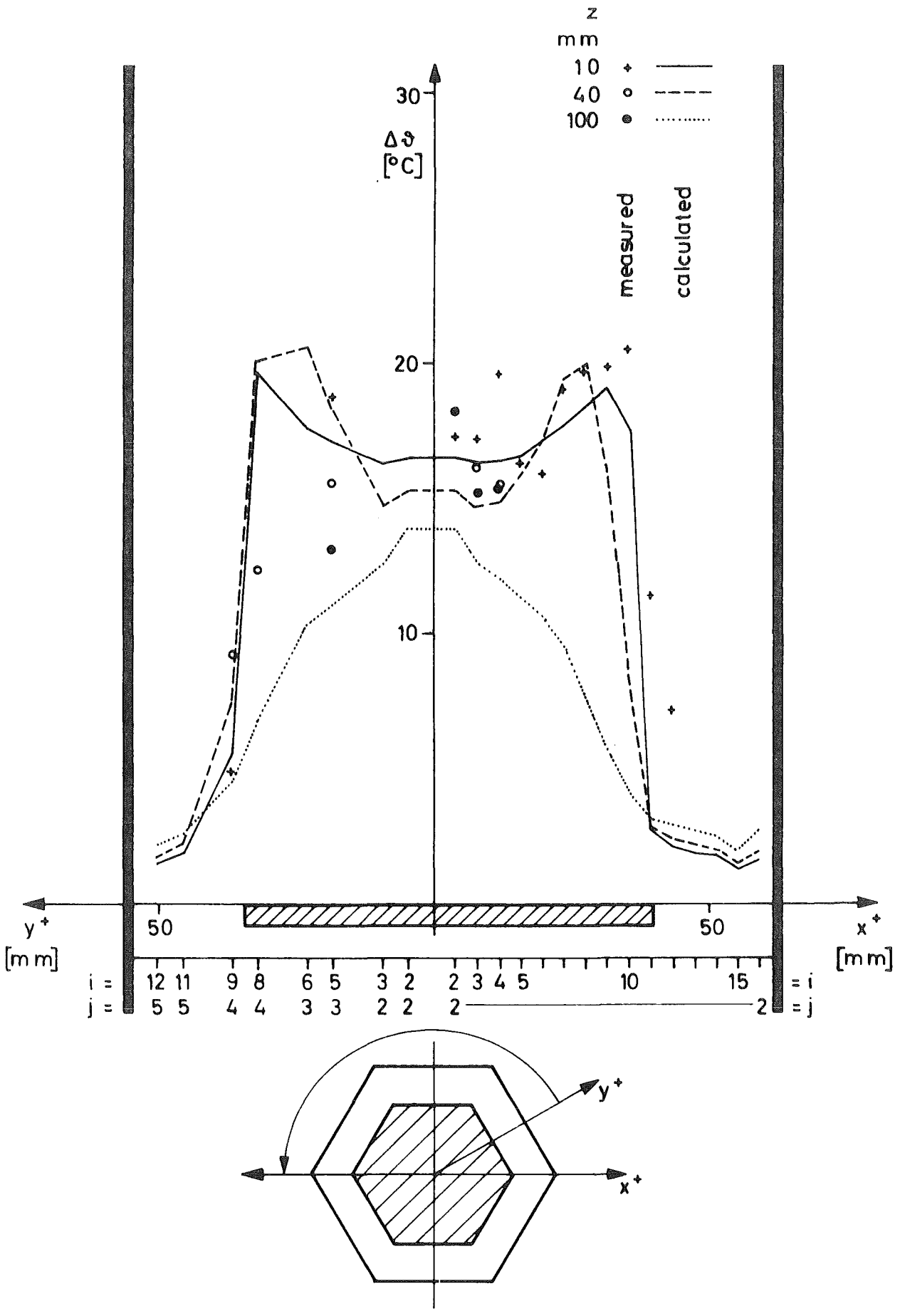

Fig. 7 Comparison of measured and calculated temperature differences for Exp. No. 41.01

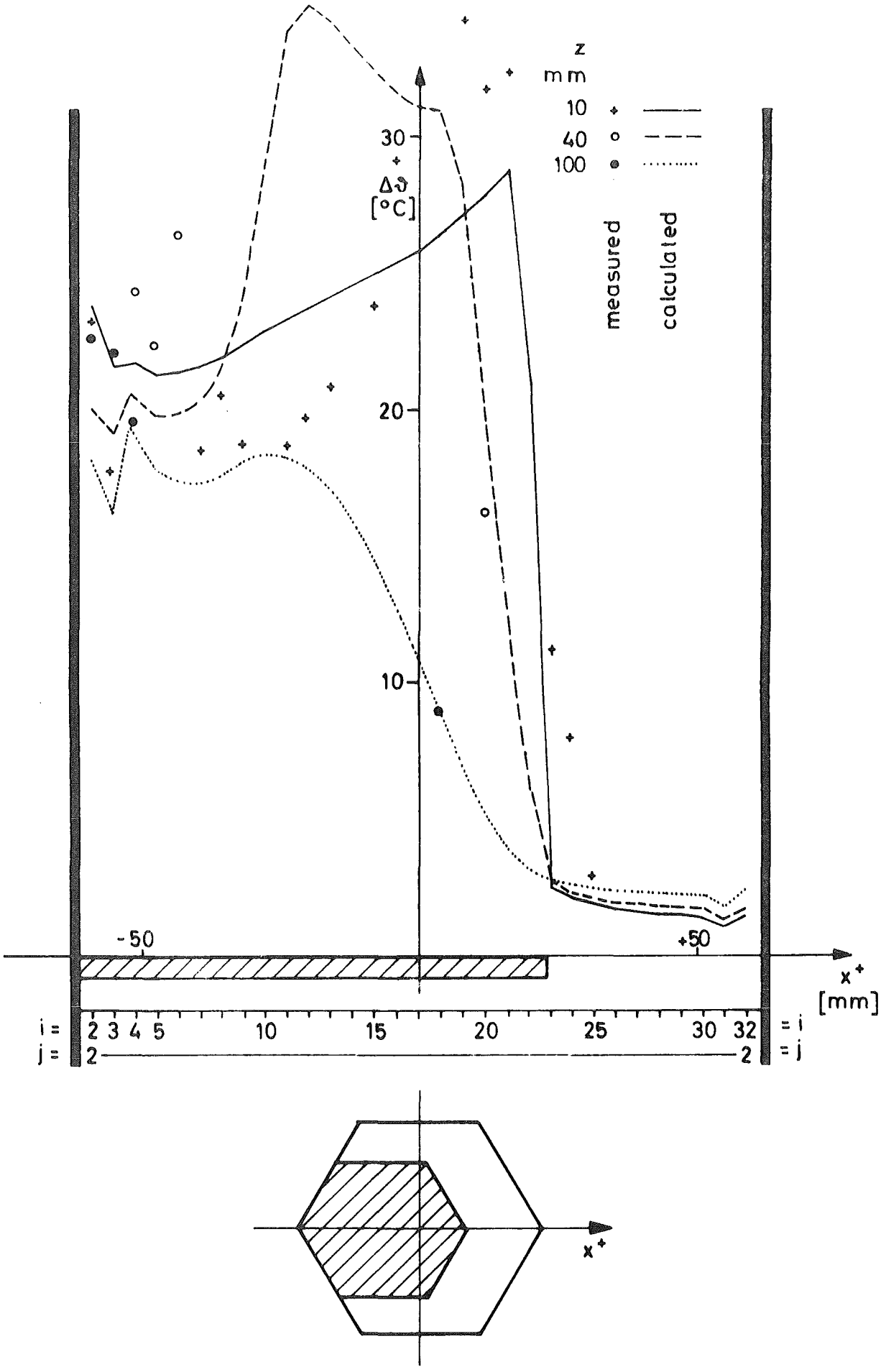

FIG. 8 COMPARISON OF MEASURED AND CALCULATED TEMPERATURE DIFFERENCES FOR EXP. No, 47.01

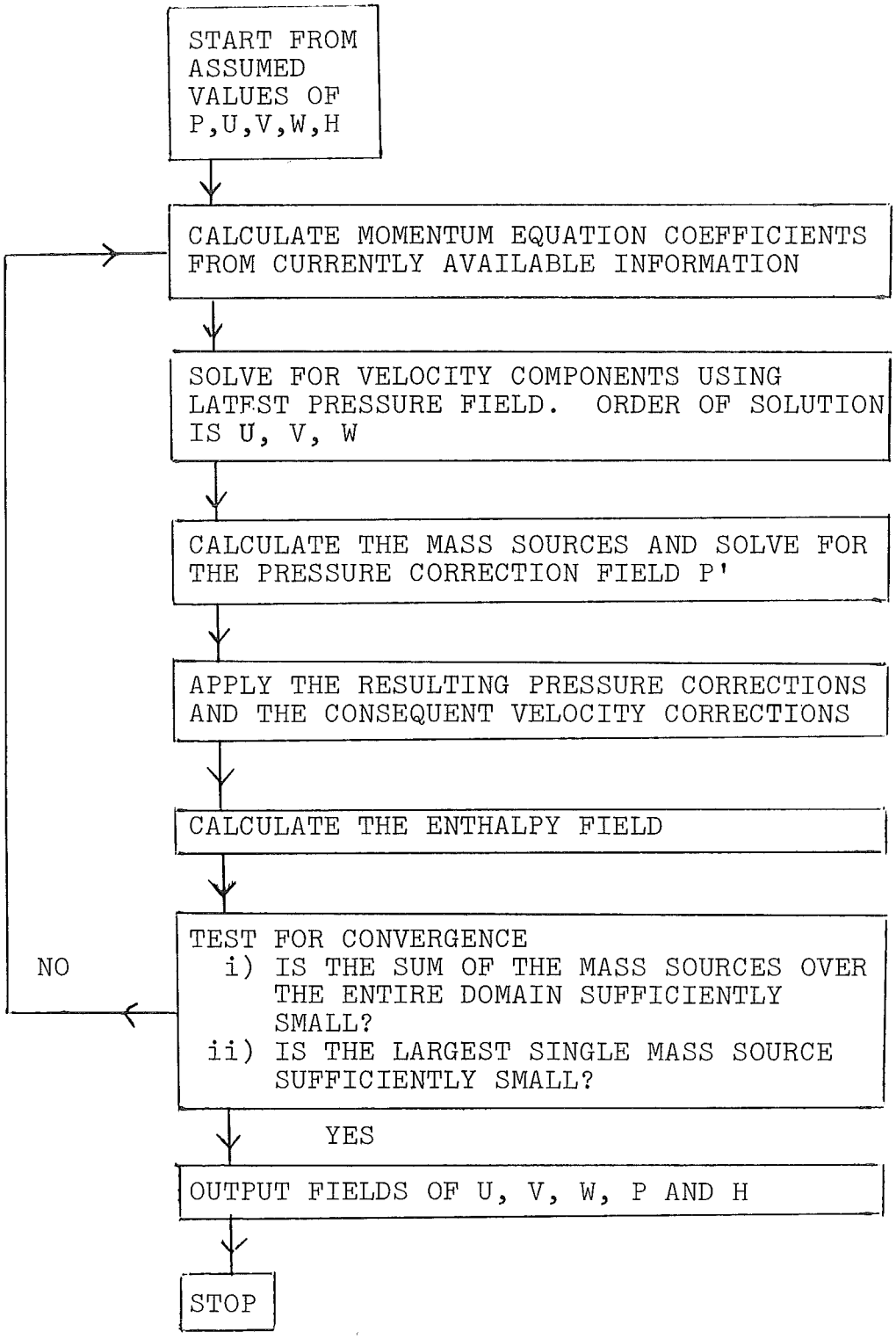

FIGURE 9 FLOW DIAGRAM OF THE SIMPLE PROCEDURE AS APPLIED IN SABRE